Journal of Scientific Research and Development 2 (13): 83-89, 2015
Available online at www.jsrad.org
ISSN 1115-7569

Numerical study on the effect of the nozzle diameter on the swirl anti-icing temperature uniformity for a nacelle lip-skin

M.A. Ismail [1, *], M.K. Abdullah [2]

[1]*Advanced Packaging and SMT group, School of Mechanical Engineering, University Sains Malaysia, Penang, Malaysia*
[2]*School of Materials and Mineral Engineering, University Sains Malaysia, Penang, Malaysia*

Abstract: The paper demonstrates the effect of the nozzle diameter on the uniformity of swirl anti-icing temperature distribution in a nacelle lip-skin. The nacelle lip-skin has been modelled using a GAMBIT pre-processor, and a FLUENT 6.0 computational fluid dynamic code is employed to obtain numerical results of the present study. The discussion covers the swirl anti-icing temperature uniformity at the hot air mass flow rate and the total temperature of 0.02531kg/m^3 and 533K, respectively. Statistical quality control and a statistical method are used to calculate the temperature deviation coefficient, as a measurement of the temperature uniformity of the swirl anti-icing system. These results show that the temperature deviation coefficient increases by 13.15%; indicating swirl anti-icing temperature uniformity quality deteriorating, as the nozzle diameter increases from 9.14mm to 25.4mm. In addition, the nacelle lip-skin average temperature also dropped by 7.5K as the average air velocity inside nacelle lip decreased from 62.7m/s to 22.0m/s.

Key words: Nozzle; Nacelle lip-skin; Swirl anti-icing; Coefficient of temperature deviation

1. Introduction

Ice accumulation is one of the key problems involving aircraft surfaces, such as the leading edges of the wings, the nacelles, the tails, etc. It affects the aerodynamic performance, contributes to high fuel consumption (Habashi, 2009), and in the worst-case scenario, leads to aircraft accidents. It has been reported that between 1982 and 2008, at least 24 aircraft accidents have been recorded due to icing, with most of them occurring during take-off and landing. Therefore, ice protection systems need to be installed on crucial aircraft surfaces, in order to prevent future aircraft crashes (Zamora, 2007).

Ice protection system is classified into two systems: De-icing {DI} and Anti-icing {AI}. A DI system is an ice protection form, in which the ice is periodically removed from the surfaces. Meanwhile, an AI system is the type of ice protection system that prevents ice accumulation at all times (Rolls-Royce, 1996). Currently, hot-air anti-icing is employed in wing and nacelle ice protection systems in commercial aircraft (Wright, 2004). Piccolo tube anti-icing {PTAI} is the most popular and efficient hot air anti-icing mechanism (Raghunathan, Benard, Watterson, Cooper, Curran, Price, Yao, Devine, Crawford, Riordan, Linton, Richardson and Tweedle, 2006). However, it causes severe temperature non-uniformity, resulting in runback ice accretion on the downstream of the outer skin (Rosenthal and Nevepovitz, 1985). Also, PTAI requires complex plumbing, and a high-density material to manufacture it, resulting in high costs and weight penalties (Ismail and Abdullah, 2015). In addition, the hotspot phenomenon may destroy the bias acoustic liner {BAL} (Elangovan, Olsen, and Reynolds, 2008).

The high temperature of the hotspots along the inner skin of the nacelle lip may cause problems and even destroy the BAL. Swirl anti-icing {SAI}, an alternative hot air anti-icing mechanism, has the potential to overcome hotspot problems. The SAI is an effective anti-icing mechanism (Herman, 1987), capable of providing uniform temperature distributions along the nacelle lip. As a result, less runback ice develops on the downstream area (Rosenthal and Nevepovitz, 1985).

The present work investigates the effect of the SAI nozzle diameter on temperature uniformity in a nacelle lip-skin. It is believed that a large nozzle diameter generates low jet velocity at a given hot air mass flow rate. As a consequence, the large nozzle produces low velocity gradient on the impingement surface, resulting in low hotspot temperature and a high degree of SAI temperature uniformity on the nacelle lip-skin. A numerical method, FLUENT 6.0 Computational Fluid Dynamic {CFD} code, is used to predict the temperature along a nacelle lip-skin. Then, Statistical Quality Control {SQC} and Statistical Method (Ismail, S.H. Mohd Firdaus, M.I. Ramdan and H. Yusoff, 2015), (Curwin and Slater, 1991), and (Kalpakjian and Schmid, 2001), are employed to measure the uniformity of temperature on a nacelle lip-skin.

* Corresponding Author.

2. Methodology

A GAMBIT pre-processor is utilized to generate a 3D-model of, and the meshing of, the nacelle lip-skin, nozzle, and air domains. A small nacelle lip, which is used for small aircraft, has a diameter of 0.6731m; hence, a D-chamber cross-sectional-area of 6.066 x $10^{-3}m^2$ is studied. In the present SAI study, the materials of the nacelle lip-skin and the nozzle are aluminium and steel, respectively. The simulation is run on a level ground, and operating conditions are shown in Table 1.

Table 1: Summary of operating conditions

Condition	Magnitude
Free stream air temperature (T_∞)	266.5K
Hot air temperature (T_n)	533.15K
Operation pressure (P_∞)	96497 Pa
Free stream velocity (v_∞)	48.75 m/s

A hexahedron with a structured grid is used in the ambient, the nacelle lip-skin, and the nozzle, in order to obtain reliable results. However, a hexahedron with hybrid grids is used in the hot air inside the nacelle lip due to the complexity of modelling and number of meshes required.

2.1. Numerical method

A three-dimensional CFD code is used to analyze the temperature distribution on a nacelle lip. The effect of six different nozzle diameters on the temperature of the nacelle lip-skin is investigated in the present work. FLUENT CFD has excellent capability to solve heat transfer problems, either in incompressible or compressible fluids, for both laminar and turbulent flows (FLUENT 6.3 User Guide, 2007). This CFD code solves equations of mass, momentum, and energy using the finite volume method. These equations rely on the following conservations:

Conservation of mass:

$$\frac{\partial \rho}{\partial t} + \frac{\delta \rho u}{\delta x} + \frac{\delta \rho v}{\delta y} + \frac{\delta \rho w}{\delta z} = 0, \quad (1)$$

Conservation of momentum:

$$\rho\left(\frac{\partial u}{\partial t} - u\frac{\partial u}{\partial x} + v\frac{\partial u}{\partial y} + w\frac{\partial u}{\partial z}\right) = -\frac{\partial P}{\partial x} + \mu\left(\frac{\partial^2 u}{\partial x^2} + \frac{\partial^2 u}{\partial y^2} + \frac{\partial^2 u}{\partial z^2}\right)$$

$$\rho\left(\frac{\partial v}{\partial t} - u\frac{\partial v}{\partial x} + v\frac{\partial v}{\partial y} + w\frac{\partial v}{\partial z}\right) = -\frac{\partial P}{\partial y} + \mu\left(\frac{\partial^2 v}{\partial x^2} + \frac{\partial^2 v}{\partial y^2} + \frac{\partial^2 v}{\partial z^2}\right)$$

$$\rho\left(\frac{\partial w}{\partial t} + u\frac{\partial w}{\partial x} + v\frac{\partial w}{\partial y} + w\frac{\partial w}{\partial z}\right) = -\frac{\partial P}{\partial z} + \mu\left(\frac{\partial^2 w}{\partial x^2} + \frac{\partial^2 w}{\partial y^2} + \frac{\partial^2 w}{\partial z^2}\right), \quad (2)$$

Conservation of energy:

$$\rho\left(\frac{\partial T}{\partial t} + u\frac{\partial T}{\partial x} + v\frac{\partial T}{\partial y} + w\frac{\partial T}{\partial z}\right) = \frac{\delta}{\partial x}\left(\frac{k}{Cp}\frac{\partial T}{\partial x}\right) + \frac{\delta}{\partial y}\left(\frac{k}{Cp}\frac{\partial T}{\partial y}\right) + \frac{\delta}{\partial z}\left(\frac{k}{Cp}\frac{\partial T}{\partial z}\right), \quad (3)$$

where ρ is the density, t is the time, u, v and w are the velocity of the flow, and x, y and z are the distance, P is the static pressure, T is the temperature, C_p is the specific heat, and k is the thermal conductivity.

The effect of body force is neglected, since the working fluid in the present study is air. This simulation assumes that the flow is compressible and fully turbulent, as the Mach number and the average Reynolds number are higher than 0.3 and 10,000 respectively. The following assumption has been made: (1) the turbulent intensity was assumed to be constant for all test conditions (turbulent intensity free stream velocity=5%, hot air inlet = 7%), and (2) the angle of attack {α} was constant for all cases (α = 0□). The turbulence model K-ω SST is selected in present study since it offers better prediction results under a severe pressure gradient, compared to the k-ε and the Spalart-Allmaras models (Bell, 2003). It was also utilized by Wong, Papadakis and Zamora (2009), and Domingos, Papadakis, and Zamora (2010) for the turbulent model in a hot-air ice protection study.

2.2. Boundary conditions

As far as the boundary conditions, shown in Fig. 1, are concerned, a pressure outlet is used on the rear surface ambient domain in order to release the free stream flow inside the ambient domain. Pressure far field (the pink-coloured cylinder surface) is utilized as the controller of the free stream velocity. The small yellow-coloured disc in the figure represents the nacelle lip and the D-chamber in the simulation. Inside the nacelle lip, as shown in Fig. 2, ten pressure outlets are used to release the exhausted hot air from the D-chamber to the ambient. These outlet surfaces are extended to prevent the backflow phenomenon inside the D-chamber. The mass-flow-rate boundary condition is utilized on the nozzle (small yellow disc in Fig. 2) inlet in order to control the total temperature and the mass-flow-rate of the hot air entering the SAI system.

3. Results and discussion

The investigation starts with a grid dependency test for obtaining reliable results, in order to determine the optimum number of meshes that will be applied. Three different numbers of meshes are tested in the present study, namely coarse mesh ($3x10^6$), fine mesh ($4.75x10^6$), and very fine mesh ($7x10^6$) in plane 0□ at the hot air mass flow rate and the total temperature of 0.01176 kg/s and 533.15K, respectively. Fig. 3 shows the point position on the nacelle lip, where the negative sign (-) represents the outer side and the positive sign (+) indicates the inner side of nacelle lip. Fig. 4 illustrates the position of the plane on the nacelle lip in the front view direction.

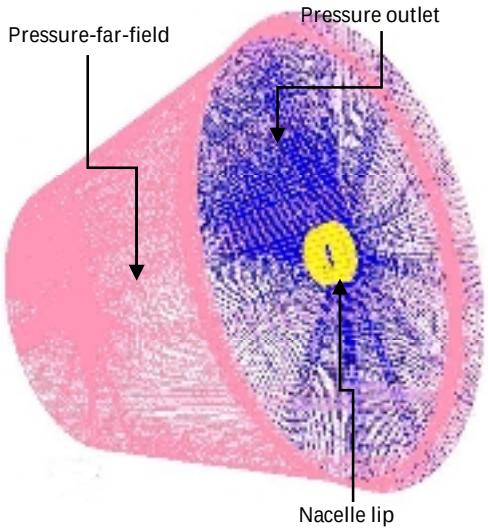

Fig. 1: Boundary condition of swirl anti-icing

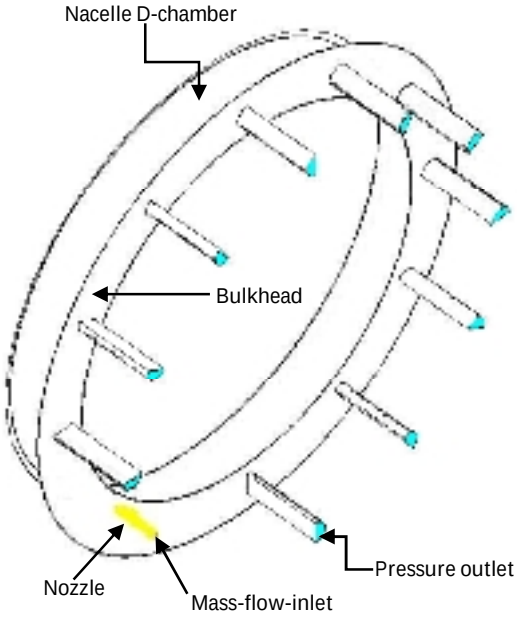

Fig. 2: Boundary condition inside nacelle lip

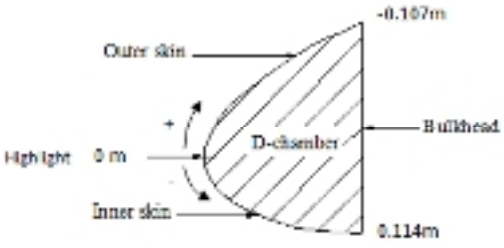

Fig. 3: Point position on the nacelle lip

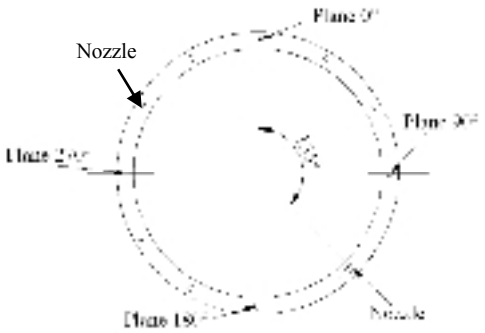

Fig. 4: Plane position on the nacelle lip

Fig. 5 reveals that the temperature distribution on the nacelle lip using very fine meshing is similar to the temperature distribution of fine meshing. However, the local temperatures of fine and very fine meshes are significantly higher than local temperatures of coarse meshing. The highest temperature deviation between fine and very fine meshing is 0.3K, which is 0.9% of the fine mesh local temperature, and it occurs at the location in the nacelle lip-skin of -0.1066m. Therefore, the fine mesh is chosen for the present study because the fine mesh only takes 14 days to converge for one case. However, the very fine mesh take 1 week longer than the fine mesh to converge for one case, while the coarse mesh is ruled out as a choice.

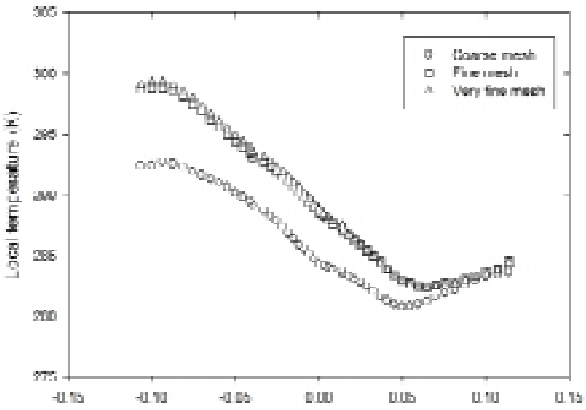

Fig. 5: Local temperature distribution (K) for various mesh density in plane 0

Afterwards, the non-dimensional wall distance {y+} of the fine mesh is examined. As shown in Fig. 6, the maximum y+ is 3.5, indicating that the first mesh spacing falls within the sub-laminar boundary layer (y+<5). As shown in Figs. 5 and 6, the fine mesh results were reliable, as the highest y+ lower than 5, as recommended by the FLUENT 6.3 User Guide (2007), and has nearly the same temperature profile as the very fine mesh.

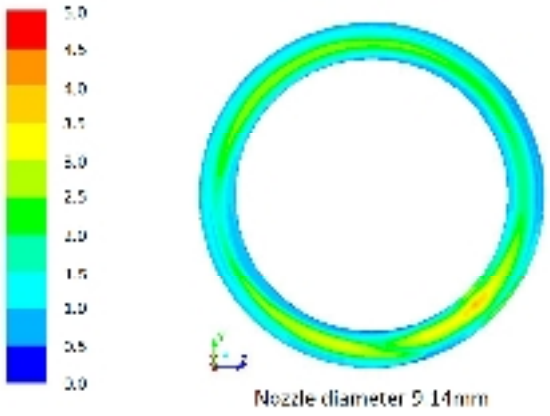

Fig. 6: Non-dimensional wall distance (y+) contour in nacelle lip-skin

Fig. 7 illustrates the comparison of temperature contours for the SAI system given two different nozzle diameters, 9.14mm and 25.4mm. The mass flow rate and the total temperature for both nozzle diameters are 0.02531kg/m^3 and 533.15K, respectively. As shown in the figure, the nozzle diameter of 9.14mm produces a more uniform temperature than the nozzle diameter of 25.4mm. The hotspot temperature of the 9.14-mm nozzle diameter is 352.3K, which is 9K lower than that of the nozzle diameter of 25.4mm. Moreover, the nozzle diameter of 25.4mm has a cold spot temperature 8.5K lower than that of the 9.14-mm nozzle diameter. The disadvantage of using the temperature contour is that it is extremely difficult to describe SAI temperature uniformity for the entire nacelle lip-skin.

The tabulation of the percentage area with regards to temperature in the nacelle lip, which is extracted from Fig. 7, is shown in Fig. 8. The objectives of the figure are to view the percentage area of the nacelle lip at a specified temperature, and to determine the temperature deviation coefficient ($C_{tem\ dev}$) in the nacelle lip-skin. As shown in the figure, for the nozzle diameter of 9.14mm, the temperatures ranging between 290K and 300K dominate 51.4% of nacelle lip-skin area. The temperature of 293K occupied 30.1% of nacelle lip-skin area, which is the largest nacelle lip-skin area coverage. For the nozzle diameter of 25.4mm, the temperature between 280K and 300K takes up over 67% of nacelle lip-skin area, where the temperature of 283K takes up the largest temperature area of the nacelle lip. The figure also shows that less than 10% of the nacelle lip-skin area is occupied by high temperatures ranging between 330K and 360K for both nozzle diameters. This phenomenon reveals that nacelle lip-skin experienced extremely non-uniform temperature distribution, especially for the nozzle diameter of 25.4mm, which has large temperature variation along the nacelle lip-skin.

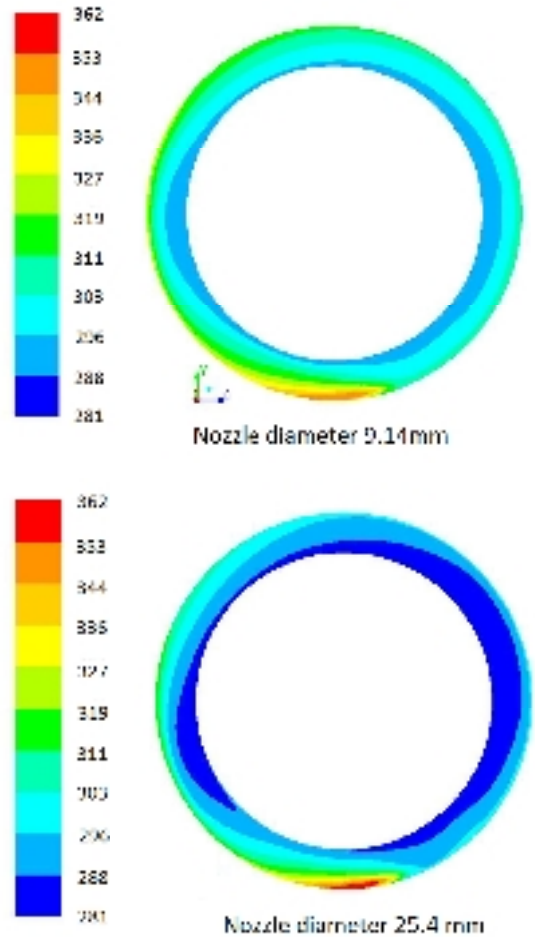

Fig. 7: Temperature contour (K) of the nacelle lip-skin for two different nozzle diameters

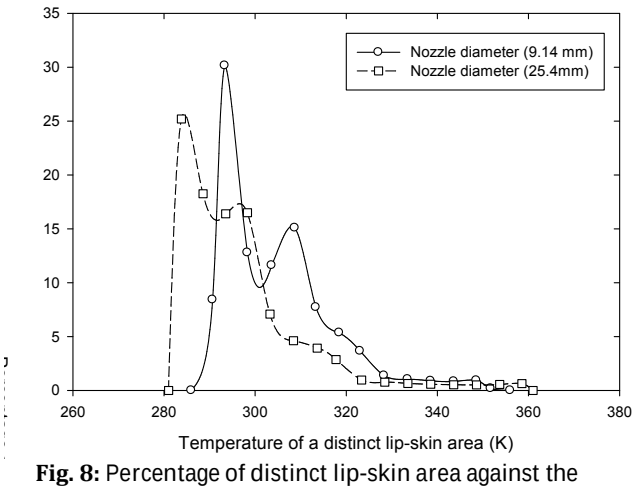

Fig. 8: Percentage of distinct lip-skin area against the temperature of a distinct lip-skin area for the entire nacelle lip-skin

The present study employs statistical quality control {SQC} and statistical method to determine $C_{tem\ dev}$, hence examining SAI temperature uniformity (Ismail, Mohd Firdaus, Ramdan and Yusoff, 2015), (Curwin and Slater, 1991), and (Kalpakjian and Schmid, 2001). Three sequence equations to

determine $C_{tem\ dev}$ are defined in Equations 4, 5, and 6.

Tave is the average temperature on the nacelle lip-skin surface:

$$T_{ave} = \frac{\sum A_{lip-skin} T_{lip-skin}}{\sum A_{totallip-skin}}, \quad (4)$$

where Alip-skin is a distinct lip skin area, or the area of a plot, Tlip-skin is the temperature of a distinct lip-skin area (Alip-skin), and Atotal lip-skin is the total lip-skin surface area.

σ is the standard temperature deviation:

$$\sigma = \sqrt{\frac{\sum A_{lip-skin}(T_{lip-skin} - T_{ave})^2}{\sum A_{totallip-skin}}} \quad (5)$$

Ctem dev is the temperature deviation coefficient:

$$C_{temdev} = \frac{\sigma}{(T_{ave} - T_{\infty})}(100) \quad (6)$$

The indicator used to describe SAI temperature uniformity in a nacelle lip-skin is the Ctem dev. A low Ctem dev stands for high SAI temperature uniformity in a nacelle lip-skin, and vice versa. The highest SAI temperature uniformity {Ctem dev is 0%} occurs when the temperature in the nacelle lip is constant for the entire surface.

Fig. 9 illustrates effect of the nozzle diameter on Ctem dev at the hot air mass flow rate and the total temperature of 0.02531kg/m3 and 522K, respectively. As shown in the figure, Ctem dev increases exponentially with the nozzle diameter, indicating that SAI temperature uniformity degrades with the nozzle diameter. According to the figure, Ctem dev increases by 13.15% as the nozzle diameter increases from 9.14mm to 25.4mm, which shows that a smaller nozzle fares better in terms of SAI temperature uniformity than a larger nozzle.

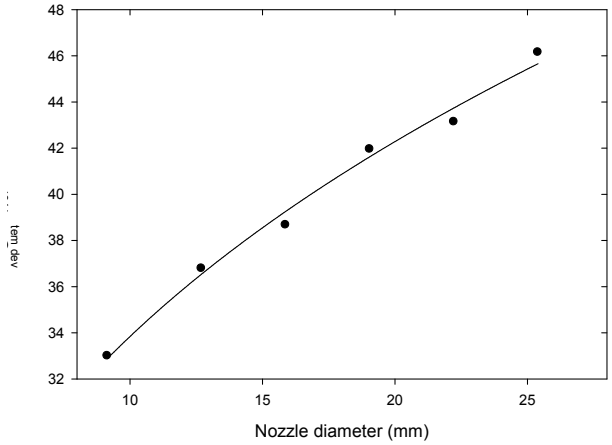

Fig. 9: Effect of nozzle diameter on coefficient of temperature deviation

At the given mass flow rate, a larger nozzle produces a lower jet velocity than a smaller nozzle. Thus, a larger nozzle should produce a less impinging effect on the surface than a smaller nozzle. As a result, a larger nozzle is supposed to produce a lower hotspot temperature and a lower $C_{tem\ dev}$ than smaller nozzle. However, according to Figs. 7 and 9, a smaller nozzle produces lower hotspot, a lower $C_{tem\ dev}$, and a higher cold spot temperature than a larger nozzle. This phenomenon happens due to two major reasons.

The first reason is the ratio of the distance between the nozzles and the impinging spot {Z} to the nozzle diameter {d} of small nozzle, being larger than that of large nozzle. In fact, the hotspot plane and the nozzle length for all nozzle diameters are similar; plane 180 and 38.1mm, respectively. Moreover, the Z for all nozzle diameters is the same, at 221mm. Thus, the Z/d of small nozzle is higher than that of a large nozzle. Table 1 shows the Z/d for all nozzle diameters.

Table 2: Z/d for nozzle diameter between 9.14mm and 25.4mm

Diameter (mm)	Z/d
9.14	24.2
12.7	17.4
15.88	13.9
19.05	11.1
22.23	9.9
25.4	8.7

The highest local heat transfer rate on the impingement surface occurs at Z/d between 5 and 7 (Raghunathan, Benard, Watterson, Cooper, Curran, Price, Yao, Devine, Crawford, Riordan, Linton, Richardson and Tweedle, 2006), then local heat transfer rate decreases as Z/d higher than 8 (Lee, Chung, and Kim, 1999). According to Table 2, the nozzle diameter of 25.4mm has a Z/d of 8.7, which is near the Z/d for the optimum local heat transfer rate. As a consequence, the nozzle with a 25.4-diameter mm has the highest local heat transfer rate and hotspot temperature on the nacelle lip surface. By contrast, the nozzle diameter of 9.14mm has the lowest hotspot temperature, since it has the largest Z/d, as illustrated in Fig. 7.

The second reason is that the jet of a smaller nozzle transfers higher momentum to the stagnation air inside the nacelle lip. Thus, a smaller nozzle produces a higher average air velocity than a larger nozzle. It is well known that a higher air velocity contributes a higher heat transfer coefficient on the surface. As a result, a smaller nozzle produces higher average temperature than a larger nozzle, which contributes to a lower $C_{tem\ dev}$ of the nacelle lip-skin (see Equation 3). This phenomenon is clearly shown in Fig. 9, where the nozzle with a 12.7-mm diameter generates a higher air velocity in the entire space inside the nacelle lip than a nozzle diameter of 22.23mm. The simulation results reveal that the average air velocity inside the nacelle lip is 46.7m/s for the nozzle diameter of 12.7mm, which is 23.9m/s higher than that of the nozzle diameter of 22.23mm.

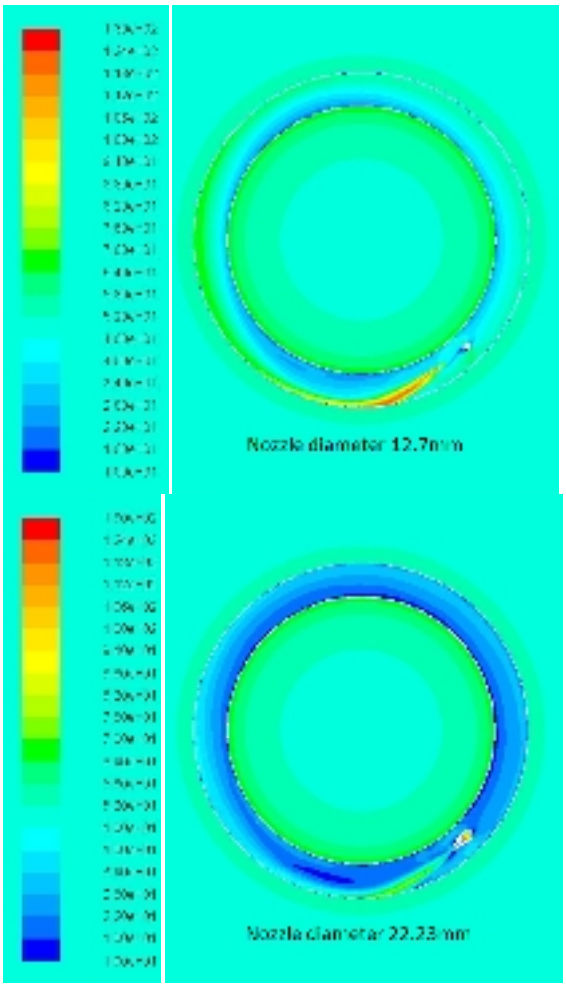

Fig. 10: The comparison of air velocity contours (m/s) between nozzle diameters of 12.7mm and 22.23mm

Table 3: The average air velocity inside the nacelle lip and the average temperature of the nacelle lip-skin

Diameter (mm)	Average air velocity inside nacelle lip (m/s)	Average lip-skin temperature (K)
9.14	62.7	303.6
12.7	46.7	301.8
15.88	37.7	300.3
19.05	30.8	298.9
22.23	25.8	297.3
25.4	22	296.2

Table 3 indicates that the average air velocity inside the nacelle lip and the average temperature of the nacelle lip-skin, was produced by SAI nozzle diameters between 9.14mm and 25.4mm. As expected, the smallest nozzle produces the highest average air velocity, and the highest average nacelle lip-skin temperature. After that, both the average air velocity and the average nacelle lip-skin temperature decrease with increasing nozzle diameter. According to the table, the nozzle diameter of 25.4mm has the lowest air velocity, and the lowest average nacelle lip-skin temperature. As all numerical data and figures show, a smaller nozzle diameter performs better in terms of SAI temperature uniformity than a larger nozzle diameter.

4. Conclusion

The purpose of this study is to investigate the effect of the nozzle diameter on the uniformity of temperature distribution on the nacelle lip-skin. We hypothesized that a large nozzle would a low hotspot temperature and $C_{tem\ dev}$. Simulation results, however, showed that a small nozzle produced a lower hotspot temperature and $C_{tem\ dev}$ than a large nozzle. According to the results, $C_{tem\ dev}$ increased by 13.25% as the nozzle diameter increased from 9.14mm to 25.4mm. In other words, a small nozzle generates better uniformity of temperature distribution than a large nozzle. That happens for two main reasons (1) a small nozzle has a larger Z/d than a large nozzle and (2) the jet from a small nozzle transfers higher momentum to the stagnation air inside nacelle lip than the jet of a large nozzle. In addition, a small nozzle provides higher average air velocity inside the nacelle lip, and a higher average nacelle lip-skin temperature than a large nozzle. At the hot air mass flow rate and the total temperature of 0.02531kg/m^3 and 522K, respectively, the average air velocity inside the nacelle lip decreases by 40.7m/s and the average temperature of nacelle lip-skin is reduced by 7.5K as the nozzle diameter increases 9.14mm to 25.4mm.

Acknowledgment

Many thanks to Grant code 304/Pmekanik/60313021 from University Sains Malaysia due to sponsored this paper.

References

A. Zamora (2007) “Numerical Investigation of Wing Hot Air Ice Protection System”, Master of Science thesis, Wichita State University, 2007.“The jet engine” Rolls-Royce 5th edition pp. 147-151, 1996.

B. Bell (2003)“Turbulent Flow Case Study”, *Fluent Software Training*, UGM, 2003.

D.H.Lee, Y.S.Chung and M.G.Kim (1999) “Technical Note Turbulent Heat Transfer from a Convex Hemispherical Surface to a Round Impinging Jet” *International Journal of Heat and Mass Transfer*, Vol. 42, No. 3, pp. 1147-1156, 1999

H.A. Rosenthal and D.O. Nevepovitz (1985) “Performance of a New Nose-Lip Hot-air Anti-Icing system", 21st Joint Propulsion Conference, Monterey, California, USA, AIAA, 1985, 85-1117.

J. Curwin and R. Slater (1991) “Quantitative Methods for Business Decisions” s.l.: Chapman and Hall, pp. 5-30, 1991

M.A. Ismail, M.Z. Abdullah “Applying Computational Fluid Dynamic to Predict the Thermal

Performance of the Nacelle Anti-Icing System in Real Flight Scenarios", *4th International Conference on Computer Science and Computational Mathematics*, May 2015.

M.A. Ismail, S.H. Mohd Firdaus, M.I. Ramdan and H. Yusoff (2015)"Numerical Investigation on Uniformity of Heat Distribution of Swirl Anti-Icing System", 4th International Conference on Computer Science and Computational Mathematics, May 2015

R. Elangovan, R.F. Olsen and N.D. Reynolds (2008) "Modelling of Acoustically Treated Nacelle Lip Transpiration Flow Anti-Icing System", 26th International Congress of the Aeronautical Sciences, 2008.

R.H. Domingos, M. Papadakis and A. Zamora (2010) "Computational Methodology for Bleed Air Ice Protection System Parametric Analysis", Atmospheric and Space Environments Conference, Toronto, Ontario Canada, 2-5 August, AIAA, 2010, 2010-7834.

R.Herman (1987) "Swirl anti-icing system", US Pattern 4688745, 1987.

S. Kalpakjian and S.R. Schmid (2001) "Manufacturing Engineering and Technology 4th edition", s.l.: Prentice-Hall, Inc., pp. 982-989, 2001 Fluent Incorporated, FLUENT 6.3 User Guide, Lebanon, NH, 2007

S. Raghunathan, E. Benard, J.K. Watterson, R.K. Cooper, R. Curran, M. Price, H. Yao, R. Devine, B. Crawford, D. Riordan, A. Linton, J. Richardson and J. Tweedle (2006)"Key aerodynamic technologies for aircraft engine nacelles", The Aeronautical Journal, Vol.110, no.17, pp.265-288, 2006.

S.H. Wong, M. Papadakis and A. Zamora (2009) "Computational Investigation of Bleed Air Ice Protection System", *1st Atmospheric and Space Environments Conference*, San Antonio, Texas, 22-25 June, AIAA, 2009, 2009-3966.

W.B. Wright (2004) "An Evaluation of Jet Impingement Heat Transfer Correlation for Piccolo Tube Application", 42nd AIAA Aerospace Science Meeting and Exhibit, 2004.

W.G. Habashi (2009) "Recent Advances in CFD for In-Flight Icing Simulation" Journal of Japan Society of Fluid Mechanics, Vol. 28 no.2, pp. 99-118, 2009.